

Nonclassical Light Generation in Two-Emitter-Cavity Systems

Marina Radulaski,* Kevin A. Fischer, Konstantinos G. Lagoudakis, Jingyuan Linda Zhang, and Jelena Vučković
E. L. Ginzton Laboratory, Stanford University, Stanford, California 94305, United States
(Dated: December 9, 2024)

Experimental developments in color center photonics are headed toward the first demonstrations of multi-emitter cavity quantum electrodynamics at the level of few emitters. We study the nonclassical light generation in such a system by extending the Tavis-Cummings model to include the influence of the inhomogeneous broadening on photon blockade. In particular, we focus on the case of $N = 2$ nonidentical quasi-atoms strongly coupled to a nanoresonator in the bad cavity regime. Bringing together the quantum master equation and the effective Hamiltonian approaches, we explain the second and third order coherence patterns and interference effects. Furthermore, we identify the conditions enabling advanced and robust single photon emission.

Introduction—Cavity quantum electrodynamics (CQED) provides a window to the quantum world where light and matter form hybridized states and enable nonclassical light generation. These experiments were initially performed with atoms in Fabry-Perot microcavities [1, 2], but their expansion to solid-state quantum dot systems represented a leap in terms of the interaction strength, increasing the emitter-cavity coupling rate g from MHz to GHz scales. This was further utilized to develop fast on-chip single photon sources [3, 4] and all-optical switches [5–7], needed for quantum cryptography and optical circuits [8]. The next step in the CQED evolution is the coupling of several ($N \gtrsim 1$) such quasi-emitters to a common nanocavity which would boost the coupling rate to $G_N \sim g\sqrt{N}$, as has been shown with atoms [9, 10]. Rare-earth ions collectively couple to cavity, but only in very large ensembles [11]. Additionally, reaching $N \gtrsim 1$ collective coupling in solid-state systems requires nearly identical emitters [12] whose inhomogeneous broadening is comparable to G_N . This is currently unreachable with ensembles of quantum dots whose frequencies spread across several THz [13].

Recently, diamond and silicon carbide color centers, which can feature inhomogeneous broadening below 30 GHz [14, 15], have been interfaced with nanocavities [16–19]. With further improvement in nanofabrication of substrates with low strain and control over emitter positioning, strong CQED coupling will be achievable at the level of several color centers. This regime [12] is characterized by the collective emitter coupling

$G_N = \sqrt{\sum_{n=1}^N g_n}$ dominating over the loss mechanisms introduced by cavity and emitter linewidths, κ and γ , respectively: $G_N > \kappa/2, \gamma/2$.

We consider theoretically the transmission through a nanocavity coupled to two nonidentical color centers, as illustrated in Fig. 1(a). Extending the Tavis-Cummings model [20] to account for individual emitter frequencies, we analyze the influence of the inhomogeneous broadening on the transmitted photon statistics. Using the quant-

um master equation [21] we calculate transmission and coherence properties, discovering conditions for photon blockade and hence for high-quality single photon emission from a multi-emitter CQED system. To understand their occurrence, we diagonalize the effective Hamiltonian and analyze the frequency overlap of the first three rungs of the dressed ladder of states. Finally, by matching the frequency difference between the excited levels and the oscillations in the second order coherence function, we identify interferences between the states that set the dynamics of the system.

The model—The interaction Hamiltonian for our CQED system consists of the cavity, emitter and coupling terms ($\hbar = 1$):

$$H_I = \omega_C a^\dagger a + \sum_{n=1}^N [\omega_{En} \sigma_n^\dagger \sigma_n + g_n (\sigma_n^\dagger a + a^\dagger \sigma_n)],$$

where a and ω_C represent the annihilation operator and resonant frequency of the cavity mode; σ_n , g_n and ω_{En} are the lowering operator, coupling strength to the cavity and transition frequency of the n -th out of $N = 2$ emitters. To treat the cavity and emitter detunings more explicitly, we rewrite emitter frequencies as $\omega_{E1} = \omega_C + \Delta_C$ and $\omega_{E2} = \omega_C + \Delta_C + \Delta_E$.

The system is characterized by the cavity energy decay and emitter linewidth [κ, γ]/ $2\pi = [25, 0.1]$ GHz, corresponding to quality factor $Q \approx 15,000$ and lifetime $\tau = 10$ ns, and the individual emitter-cavity coupling

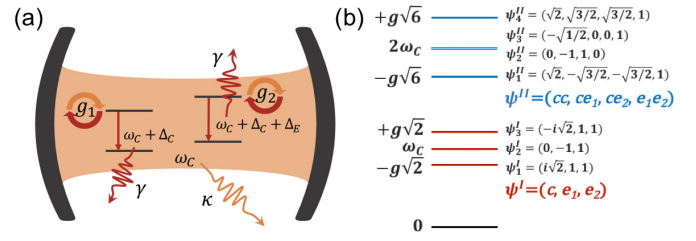


FIG. 1. (a) An illustration of the multi-emitter CQED system with two nonidentical emitters coupled to a common cavity mode. (b) The ladder of dressed states, frequencies and unnormalized eigenvectors, for the case of two identical and equally coupled emitters, $\Delta_C = \Delta_E = 0$ and $g_1 = g_2 = g$.

* marina.radulaski@stanford.edu

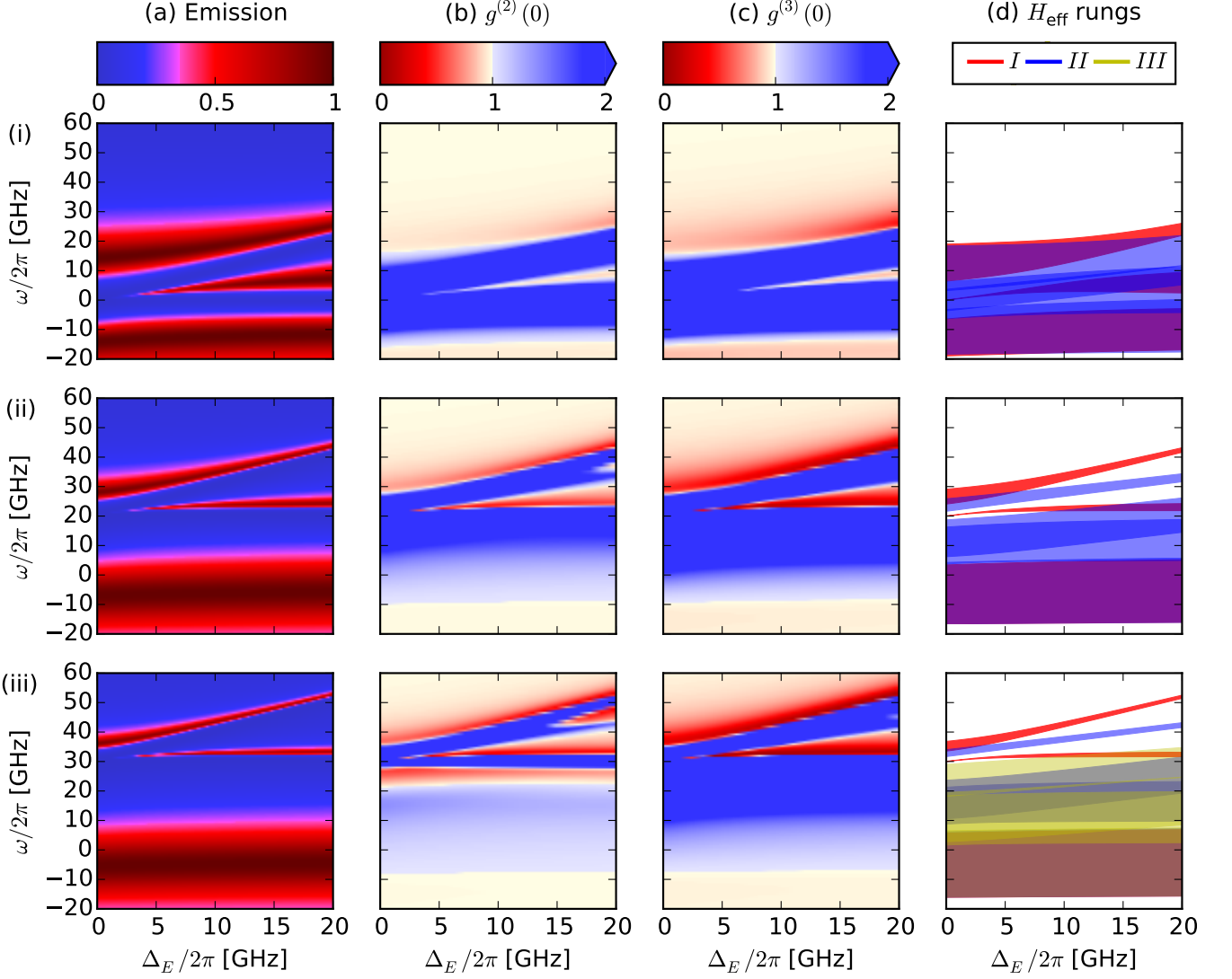


FIG. 2. (a) Emission spectrum, (b) second and (c) third order coherence of transmitted light calculated by the quantum master equation. (d) Frequency overlap between the rungs of the dressed ladder of states of H_{eff} , presented as $\omega_n/n - \omega_C$ with indicated linewidths; $\Delta_C/2\pi$ takes values of (i) 0, (ii) 20 and (iii) 30 GHz.

rate of $g_n/2\pi = 10$ GHz. Comparing to the state-of-the-art results [19] with silicon-vacancy centers in a photonic crystal cavity, the quoted values could be achieved by designing nanocavities with twice the quality factor and several times smaller mode volume, while simultaneously providing more precise positioning of the color center at the field maximum [22], to achieve five-fold increase in the coupling rate. The threefold mismatch in emitter linewidth, which is the smallest rate in the system, can be tolerated in the bad cavity regime. With the imposed set of parameters, a single emitter would be weakly coupled to the cavity ($g_n < \kappa/2$), however, the collective coupling of two emitters brings the system into the strong coupling regime ($\sqrt{g_1^2 + g_2^2} > \kappa/2$).

To model the interaction of the system with its environment, we use the quantum master equation to calcu-

late the steady state solution of the density matrix ρ :

$$\dot{\rho} = -i[H_I + E_P(ae^{i\omega t} + a^\dagger e^{-i\omega t}), \rho] + \kappa L[a] + \sum_{n=1}^N \gamma_n L[\sigma_n],$$

where $E_P = \kappa/50$ is the laser field amplitude, and loss terms are introduced through the Lindblad superoperator $L[O] = O\rho(t)O^\dagger - \frac{1}{2}\rho(t)O^\dagger O - \frac{1}{2}O^\dagger O\rho(t)$. The steady state solution is found after transformation to a rotating frame to remove the time-dependence [23]. When obtaining emission spectra, we leave the E_P term out and add a pump term in the Liouvillian as $PL[a^\dagger]$, where P represent the laser power.

We gain a more intuitive understanding of the system dynamics by diagonalizing the effective Hamiltonian, constructed with the complex frequencies that account

for cavity and emitter loss [12]. The dynamics of the first rung of the dressed ladder is represented by the operator:

$$H_{\text{eff}}^I = \begin{bmatrix} \omega_C - i\frac{\kappa}{2} & g_1 & g_2 \\ g_1 & \omega_{E1} - i\frac{\gamma}{2} & 0 \\ g_2 & 0 & \omega_{E2} - i\frac{\gamma}{2} \end{bmatrix}.$$

The real and the imaginary part of its eigenvalues represent frequencies and half-linewidths of the excited energy states, respectively, while the eigenvectors quantify the cavity-like and the emitter-like character of the excited state. Figure 1(b) shows the eigenfrequencies and eigenvectors in the ladder of dressed states for an identical and equally coupled system. The eigenvector elements are labeled with c for cavity, e_1 and e_2 for the first and the second emitter excitation, respectively. Comparing to a single emitter in a cavity, where all excited states contain two levels, we immediately see that an additional emitter generates more excited states. The new middle state in the first rung resembles the wavefunction of a subradiant state $(e_2 - e_1)/\sqrt{2}$, known from atomic systems to not couple to the environment. There are also two new middle states in the second rung, which are degenerate for this set of detunings. These additional levels ultimately lead to a much richer set of physics phenomena. Not only do we find an enhanced regime of photon blockade from the subradiant states, but a newly discovered un-conventional photon blockade regime [24] can also be achieved in the system. We now explore these effects as a function of the emitter detuning Δ_E .

Results—We present calculation results for cavity detunings $\Delta_C/2\pi = 0, 20$ and 30 GHz which capture system's trends and features. The emission spectra are shown in Fig. 2(a). In parallel, we calculate the eigenstates of the first rung of the effective Hamiltonian, shown as red surfaces in Fig. 2(d). The three transmission peaks are in a close agreement with the eigenfrequencies of H_{eff}^I , with the bottom peak being cavity-like, and the top two peaks emitter-like. For small Δ_E the system exhibits a combination of effects of the strong emitter-cavity coupling, and of an emergent subradiant state. Similar spectra have been derived for superconducting cavities coupled to an ensemble of spins [25] and experimentally observed in superconducting circuits [26]. The strong coupling rate is $G_2 = \sqrt{g_1^2 + g_2^2}$ and the spectrum consists of two polaron peaks with frequencies close to $\omega_{\text{pol}\pm}^{\Delta_E=0} = \omega_C + \frac{\Delta_C}{2} - i\frac{\kappa+\gamma}{4} \pm \frac{\sqrt{4\Delta_C^2 + 16G_2^2 + 2\kappa\gamma + 4i\Delta_C\kappa - 4i\Delta_C\gamma + i\kappa^2 + i\gamma^2}}{4}$. We derive an approximation to the subradiant state frequency ω_{sub} and vector v_{sub} for $\Delta_E \ll G_2, \frac{\kappa-\gamma}{2}$:

$$\omega_{\text{sub}} = \omega_C + \Delta_C + \frac{g_1^2}{G_2^2} \Delta_E - i \left(\frac{\gamma}{2} + \frac{\kappa - \gamma}{8G_2^2} \Delta_E^2 \right),$$

$$v_{\text{sub}} = \frac{1}{\sqrt{A}} \begin{bmatrix} -\frac{g_2 \Delta_E}{G_2^2} + i \frac{\kappa - \gamma}{8g_2} \frac{\Delta_E^2}{G_2^2} \\ -\frac{g_1}{g_2} \frac{8g_2^2 + i(\kappa - \gamma)\Delta_E}{8g_1^2 - i(\kappa - \gamma)\Delta_E} \\ 1 \end{bmatrix},$$

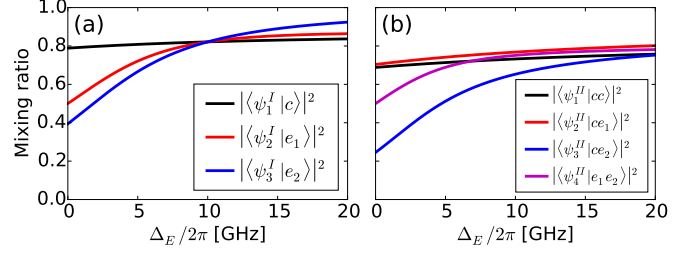


FIG. 3. Prevalent character of the eigenstates of (a) the first and (b) the second rung of H_{eff} for $\Delta_C = 20$ GHz.

where A is a normalization factor. For vanishing Δ_E the cavity term in v_{sub} becomes zero, meaning the state does not couple to the environment. With an increasing Δ_E , the frequency of the subradiant state grows linearly, while the linewidth and the amplitude increase quadratically, closely matching the trend in the simulated emission spectra for $\Delta_E/2\pi \leq 3$ GHz.

Next, we analyze the second order coherence of light transmitted through the system, shown in Fig. 2(b). Focusing on the (red) areas with suppressed two photon statistics $g^{(2)}(0) < 1$, we notice that their occurrence correlates with the emission peaks, which is especially prominent for the upper two peaks at moderate and large Δ_E . Looking into the frequency overlap of the first (red) and second (blue) rung in Fig. 2(d), we see that the two photon emission is suppressed in the areas where single photon absorption is possible, but the second photon does not have a spectrally close state to be absorbed at (no overlapping blue areas). This is in line with results obtained in single emitter CQED systems, where photon blockade was improved for larger emitter-cavity detunings [3]. However, we also notice that the transmission through the middle peak at large Δ_E , despite having an overlapping state in the second rung, still exhibits a suppressed two-photon transmission. To understand this, we perform an additional analysis of the eigenstate character for $\Delta_C/2\pi = 20$ GHz, presented in Fig. 3. We find that for an increasing Δ_E eigenstates $\psi_1^I, \psi_2^I, \psi_3^I, \psi_1^{II}, \psi_2^{II}, \psi_3^{II}$ and ψ_4^{II} prevalently exhibit $c, e_1, e_2, cc, ce_1, ce_2$, and e_1e_2 character, respectively. The dipolar coupling between ψ_2^I and ψ_3^{II} has to be inhibited due to $\langle ce_2 | a^\dagger | e_1 \rangle = 0$, which explains the suppression of the second photon absorption at the higher detunings, despite their frequencies overlap. Single-photon character is further confirmed by the third order coherence plots in Fig. 2(c), where we observe three photon statistic suppression in the same areas. With this combination of spectral and vector orthogonality properties obtained from the diagonalization of the effective Hamiltonian we predict parameters that give rise to enhanced single photon emission. The properties also hold for nonidentically coupled emitters ($g_1 \neq g_2, G_2 > \kappa/2$), which has practical implications for systems with randomly positioned color centers whose coupling strength can not be imposed uniformly.

In addition to these trends, we observe that in the case

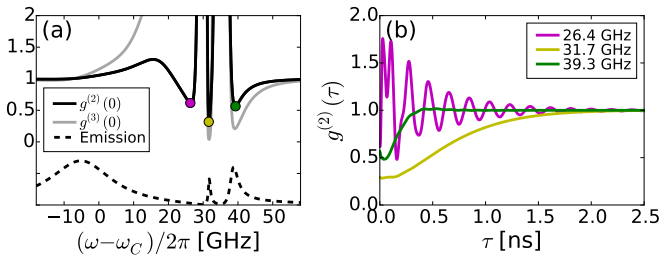


FIG. 4. (a) Zero-delay second and third order coherences for $[\Delta_C, \Delta_E]/2\pi = [30, 5]$ GHz system as a function of laser detuning from the cavity; emission spectrum is plotted in dashed lines to illustrate the correlation between features. (b) $g^{(2)}(\tau)$ at frequencies of the corresponding $g^{(2)}(0)$ minima from (a).

of $\Delta_C/2\pi = 30$ GHz the region around $\omega/2\pi = 25$ GHz has low $g^{(2)}(0)$ but high $g^{(3)}(0)$. A similar superbunching behavior has recently been predicted for systems with third-order nonlinearity and dubbed *unconventional photon blockade* [24], proving that reduction in $g^{(2)}(0)$ value is not a sufficient criterion for single photon emission. To understand the occurrence of this regime in our system, we look into the third rung of the dressed ladder shown in yellow at Fig. 2(d-iii). We see that these frequencies have an overlapping three-photon absorbing state, but no two-photon absorbing state, which explains the calculated statistics whereby the system preferentially emits groups of three photons at this frequency. Thus the multi-emitter CQED system will not just enhance single-photon blockade, but also allow for the exploration of exciting regimes of multi-photon physics and statistics.

Finally, we analyze the system dynamics in the time domain, on an example of $[\Delta_C, \Delta_E]/2\pi = [30, 5]$ GHz which has three $g^{(2)}(0)$ dips, presented in Fig. 4(a). The second order coherence evolution at the frequency of the dip which exhibits un-conventional blockade, shown in blue in Fig. 4(b), represents a damped oscillation and once again confirms the system at these frequencies can not be a good single photon source. The dominant oscillation frequency ($\omega/2\pi$) is 5.2 GHz, while the first 200 ps also exhibit additional 11 GHz oscillation. The other two second order coherence traces are at frequencies of conventional photon blockade, and represent a decay to a coherent state. The characteristic half-width at half-maximum times are 0.7 ns and 0.2 ns for the transmission through states with e_1 (yellow) and e_2 (green) characters, respectively, and represent a speedup in single photon emission compared to bare quasi-emitter. Both functions exhibit 44 GHz oscillations with small amplitudes in the first 200 ps, which corresponds to the frequency

difference between top and bottom eigenstates in the first rung of the dressed ladder shown in 2(d-iii), analogous to the interference between polariton states experimentally observed in single atom-cavity systems [27]. The function plotted in green also oscillates at 7.7 GHz at longer times, whose origin we assign to the interference between the upper two states in the first rung. We observe this trend for other sets of parameters as well.

Discussion—Comparing nonclassical light generation in our $N = 2$ multi-emitter-cavity system with $N = 1$ case [3], we both predict lower values of $g^{(2)}(0)$ and find opportunities for more robust single photon generation. The frequency and the second order coherence values of light transmitted through the state ψ_2^I are close to constant for given cavity detuning. Experimentally, this means that for any pair of nonidentical emitters (3 GHz $\leq \Delta_E/2\pi \leq 20$ GHz) the quality of single photon emission is dictated by the cavity detuning from the first emitter. Experimentally, this variable can be controlled by gas tuning techniques without influencing the operating laser frequency.

In conclusion, we have analyzed nonclassical light generation in a strongly coupled two-emitter CQED system for variable cavity and emitter detuning. Combining quantum master equation and effective Hamiltonian approaches, we identified the parameters that give rise to robust photon blockade, and explained their origin in the overlap between the eigenstates of multiple rungs of the dressed ladder of states. We also characterized the oscillations in $g^{(2)}(\tau)$ function as interference between the states of the first rung. The time scale of the single photon emission represents an order of magnitude speedup over the bare emitter dynamics, while the $g^{(2)}(0)$ values are improved over the system with a single emitter in a cavity. In light of the presented opportunities in conventional and un-conventional photon blockade, multi-photon emission and operating rate speedup, we expect that $N > 2$ multi-emitter CQED systems will unveil even richer physics. For systems with more than several emitters, numerical calculations may prove lengthy due to the large size of the density matrix, however, our theoretical analysis based on the diagonalization of the effective Hamiltonian can provide a quick insight into the potential parameter areas with robust single photon emission.

Acknowledgements—This work has been supported by the National Science Foundation (DMR Grant Numbers 1406028 and 1503759). We thank Hideo Mabuchi, Nikolas Tezak and Dmitri Pavlichin for constructive discussions. K.A.F. acknowledges support from the Lu Stanford Graduate Fellowship and the National Defense Science and Engineering Graduate Fellowship.

[1] S. Haroche and D. Kleppner, Phys. Today **42**, 24 (1989).
[2] K. M. Birnbaum, A. Boca, R. Miller, A. D. Boozer, T. E. Northup, and H. J. Kimble, Nature **436**, 87 (2005).
[3] K. Müller, A. Rundquist, K. A. Fischer, T. Sarmiento, K. G. Lagoudakis, Y. A. Kelaita, C. S. Muñoz, E. del Valle, F. P. Laussy, and J. Vučković, Physical review

letters **114**, 233601 (2015).

- [4] C. P. Dietrich, A. Fiore, M. G. Thompson, M. Kamp, and S. Höfling, *Laser & Photonics Reviews* (2016).
- [5] A. Majumdar, M. Bajcsy, D. Englund, and J. Vuckovic, *IEEE Journal of Selected Topics in Quantum Electronics* **18**, 1812 (2012).
- [6] H. Kim, R. Bose, T. C. Shen, G. S. Solomon, and E. Waks, *Nature Photonics* **7**, 373 (2013).
- [7] T. Volz, A. Reinhard, M. Winger, A. Badolato, K. J. Hennessy, E. L. Hu, and A. Imamoglu, *Nature Photonics* **6**, 605 (2012).
- [8] J. L. O'Brien, A. Furusawa, and J. Vučković, *Nature Photonics* **3**, 687 (2009).
- [9] R. Thompson, G. Rempe, and H. Kimble, *Physical Review Letters* **68**, 1132 (1992).
- [10] A. Neuzner, M. Körber, O. Morin, S. Ritter, and G. Rempe, *Nature Photonics* **10**, 303 (2016).
- [11] T. Zhong, J. M. Kindem, J. Rochman, and A. Faraon, arXiv preprint arXiv:1604.00143 (2016).
- [12] I. Diniz, S. Portolan, R. Ferreira, J. Gérard, P. Bertet, and A. Auffeves, *Physical Review A* **84**, 063810 (2011).
- [13] D. Gammon, E. Snow, B. Shanabrook, D. Katzer, and D. Park, *Science* **273**, 87 (1996).
- [14] A. Sipahigil, K. D. Jahnke, L. J. Rogers, T. Teraji, J. Isoya, A. S. Zibrov, F. Jelezko, and M. D. Lukin, *Physical review letters* **113**, 113602 (2014).
- [15] P. G. Baranov, A. P. Bundakova, A. A. Soltamova, S. B. Orlinskii, I. V. Borovskykh, R. Zondervan, R. Verberk, and J. Schmidt, *Physical Review B* **83**, 125203 (2011).
- [16] B. Hausmann, B. Shields, Q. Quan, Y. Chu, N. De Leon, R. Evans, M. Burek, A. Zibrov, M. Markham, D. Twitchen, *et al.*, *Nano letters* **13**, 5791 (2013).
- [17] M. Radulaski, Y.-K. Tzeng, J. L. Zhang, K. G. Lagoudakis, H. Ishiwata, C. Dory, K. Alassaad, G. Ferro, Z.-X. Shen, N. Melosh, *et al.*, arXiv preprint arXiv:1610.03183 (2016).
- [18] D. O. Bracher and E. L. Hu, *Nano letters* **15**, 6202 (2015).
- [19] A. Sipahigil, R. Evans, D. Sukachev, M. Burek, J. Borregaard, M. Bhaskar, C. Nguyen, J. Pacheco, H. Atikian, C. Meuwly, *et al.*, *Science* **354**, 847 (2016).
- [20] M. Tavis and F. W. Cummings, *Physical Review* **170**, 379 (1968).
- [21] M. Orszag, *Quantum optics: including noise reduction, trapped ions, quantum trajectories, and decoherence* (Springer, 2016).
- [22] T. Schröder, M. E. Trusheim, M. Walsh, L. Li, J. Zheng, M. Schukraft, J. L. Pacheco, R. M. Camacho, E. S. Bielejec, A. Sipahigil, *et al.*, arXiv preprint arXiv:1610.09492 (2016).
- [23] D. A. Steck, University of Oregon (2007).
- [24] J. C. L. Carreño, E. Z. Casalengua, E. del Valle, and F. P. Laussy, arXiv preprint arXiv:1610.06126 (2016).
- [25] R. Houdré, R. Stanley, and M. Illegems, *Physical Review A* **53**, 2711 (1996).
- [26] J. Fink, R. Bianchetti, M. Baur, M. Göppl, L. Steffen, S. Filipp, P. Leek, A. Blais, and A. Wallraff, *Physical review letters* **103**, 083601 (2009).
- [27] M. Koch, C. Sames, M. Balbach, H. Chibani, A. Kubanek, K. Murr, T. Wilk, and G. Rempe, *Physical review letters* **107**, 023601 (2011).